Available online at www.sciencedirect.com

ScienceDirect

IFAC PapersOnline CONFERENCE PAPER ARCHIVE

IFAC PapersOnLine 52-15 (2019) 157–162

Data-based feedback controller tuning utilizing collocated and non-collocated sensors ⋆

Wataru Ohnishi *

* *The University of Tokyo, 7-3-1 Hongo, Bunkyo-ku, Tokyo, 113-8656, Japan, ohnishi@koseki.t.u-tokyo.ac.jp*

Abstract: In motion control applications, such as machine tools and high-precision positioning stages for the semiconductor or flat panel industries, it is becoming common to place sensors on not only the motor side (collocated side) but also the load side (non-collocated side). The load side information enables compensation of transmission dynamics, such as friction or backlash. However, due to the phase lag of the load side frequency characteristics, it is difficult to increase the feedback bandwidth. To address this problem, this paper proposes a feedback controller design method based on frequency response data that utilizes both collocated and non-collocated sensor information. Experimental results show that the proposed method effectively suppresses the input disturbance. Furthermore, the proposed optimization requires less calculation time compared with nonlinear optimization with random initial values and exhibits better performance.

Keywords: Additional sensor, Concave-convex procedure, Data based tuning, Frequency responses

1. INTRODUCTION

In high-precision motion control systems, such as machine tools and positioning stages for the semiconductor or flat panel industries, it is becoming increasingly common to place sensors on not only the driving side (collocated side) but also the load side (non-collocated side) (Sakata et al., 2014; Oomen, 2018). There are two common ways to close the feedback (FB) loop, namely semi-closed loop control and full-closed loop control (Yamaguchi et al., 2011). The semi-closed loop control system feeds back the sensor information only from the motor side, while the full-closed loop control system feeds back the sensor information from the motor side as well as from the load side (Hu et al., 2014), which is located close to the point of interest (Butler, 2011). The full-closed loop control system generally shows better performance, especially in the steady-state because it feeds back information that includes transmission part dynamics, such as friction or backlash. However, it is difficult for the full closed-loop control to have a high feedback bandwidth because the information from the load side (non-collocated side) contains a phase lag (Hara et al., 2008).

Herein, a method called self-resonance cancellation (SRC), which aims to achieve high-feedback bandwidth by utilizing both collocated and non-collocated sensor information, is proposed (Sakata et al., 2014). In short, this method 1) models the system as a fourth order system that contains a rigid body mode and first resonance mode, 2) calculates the center of gravity position by interior division of the two sensors ("resonance cancellation"), and 3) designs a high-bandwidth feedback controller for an imaginary system without the first resonance mode. However, this method does not ensure position accuracy of the load side because it does not directly feedback the load side information. To address this problem, the method is extended to a complementary filter-based method (Sakata et al., 2014) and SRC-P-PI control (Hasegawa et al., 2017). The SRC-P-PI control has an inner proportional-integral (PI) velocity feedback with SRC and an outer proportional (P) position feedback. However, the above methods need a parametric model including the first resonance and they do not explicitly discuss design methods with multiple resonances.

Feedback controller tuning methods based on frequency response data, such as the Ziegler–Nichols method, have been extensively studied (Ziegler and Nichols, 1942; Åström and Murray, 2008). Furthermore, optimization-based tuning methods, such as the genetic algorithm (Tang et al., 2001), Nelder–Mead method (Lee et al., 1985), and particle swarm optimization (Gaing, 2004), have been proposed. Convex optimization-based methods for a fixed structure controller have been proposed, including an open loop shaping method using a desired open loop transfer function (Karimi and Galdos, 2010) and a sequential linearization method using the concave-convex procedure (CCCP) (Hast et al., 2013; Nakamura et al., 2016). For the above mentioned methods, there are only limited discussions on how to utilize both collocated and non-collocated sensor information to design fixed structure controllers.

This paper proposes a feedback controller tuning method with high disturbance suppression performance for a system with collocated and non-collocated sensors. The proposed method requires the following information: 1) single input double output frequency response data and 2) rigid body model (nominal mass and damping coefficient). The proposed controller has a cascaded structure with a collocated side PI velocity controller with SRC and a non-collocated side P position controller. It has four non-affine tuning parameters optimized through the 1) pole-placement method, 2) sequential linearization (CCCP) method, and 3) Nelder–Mead method.

In general, nonlinear optimization problems have strong initial value dependence. We also demonstrate that the proposed method achieves higher performance with shorter calculation

⋆ I would like to thank Prof. Fujimoto for his help with the experimental setup. This work was supported by JSPS KAKENHI Grant Number 18H05902.

10.1016/j.ifacol.2019.11.667

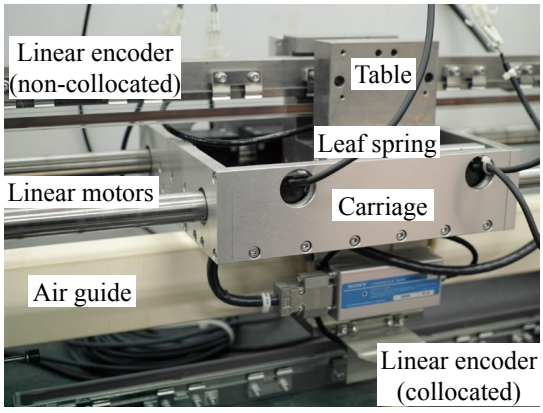

Fig. 1. High-precision positioning stage (Hara et al., 2008).

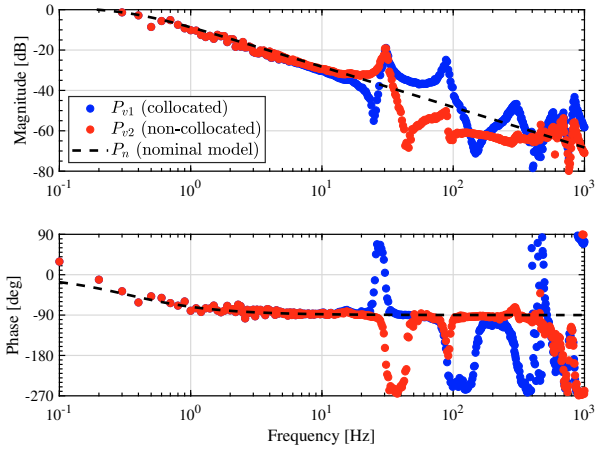

Fig. 2. Frequency response of the plant (input current to velocities). The frequency response data and first order nominal model P_n are used for controller design.

time than the Nelder–Mead method with 1000 pattern randomly selected initial values. This paper also compares the proposed method with proportional-integral-derivative (PID) control for the non-collocated position to show the effectiveness of the SRC-P-PI control structure. The PID gains and the time constant of pseudo difference are optimized similar to the proposed procedure: 1) pole-placement method, 2) sequential linearization method, and 3) Nelder–Mead method. Note that the PID controller has four tuning parameters, which is the same number of tuning parameters as that for SRC-P-PI control.

2. EXPERIMENTAL SETUP

A one-axis high-precision positioning stage, as shown in Fig. 1, is used as an experimental setup. The input is a pair of linear motors at the carriage. The output is two encoders located at the carriage and table. There is a spring between the carriage and table. Therefore, the encoder at the carriage is a collocated side sensor, and the encoder at the table is a non-collocated side sensor. Here, the point of interest is assumed as the table side position.

Frequency responses from the input current to both the sides' velocities are shown in Fig. 2. This is obtained through frequency domain identification (Pintelon and Schoukens, 2012). The collocated side response P_{v1} has an anti-resonance first and a resonance later. In contrast, the non-collocated side response P_{v2} has a resonance first followed by an anti-resonance.

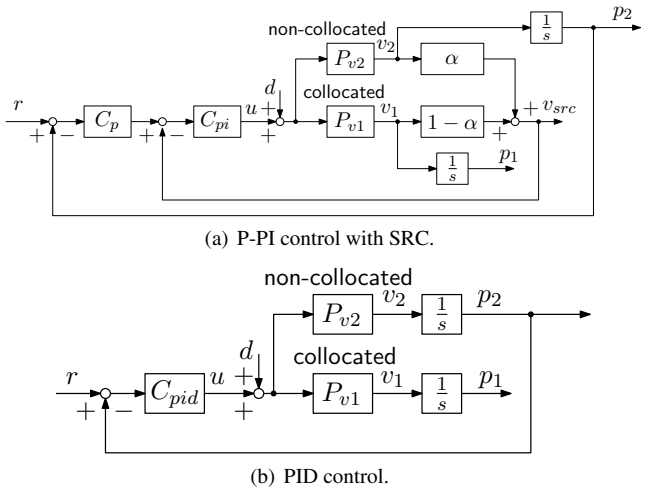

(a) P-PI control with SRC.

(b) PID control.

Fig. 3. Block diagrams of the compared controller configurations.

A first-order nominal model P_n is

$$P_n(s) = \frac{1}{M_n s + B_n} \tag{1}$$

$$M_n = 0.412,\ B_n = 0.866. \tag{2}$$

3. SRC-P-PI CONTROLLER DESIGN

In this section, the proposed SRC-P-PI controller design using frequency response data is described. The block diagram representation is shown in Fig. 3(a).

The transfer function of the plant with SRC is

$$P_{vsrc}(j\omega_k, \alpha) = (1-\alpha)P_{v1}(j\omega_k) + \alpha P_{v2}(j\omega_k), \tag{3}$$

where ω_k and k denote the measured frequency point and the data number, respectively. Hence, the open loop transfer function is represented by

$$L_{vsrc}(j\omega_k, \boldsymbol{\rho}, \alpha) = [(1-\alpha)\ \ \alpha]\begin{bmatrix} P_{v1}(j\omega_k) \\ P_{v2}(j\omega_k) \end{bmatrix}[k_{vp}\ \ k_{vi}]\begin{bmatrix} 1 \\ \dfrac{1}{j\omega_k} \end{bmatrix}, \tag{4}$$

where $\boldsymbol{\rho} = [k_{vp},\ \ k_{vi}]^\top$ denotes the PI gain. It is not affine for $\boldsymbol{\rho}$ and α; therefore, the linear optimization is not applicable. Hence, the pole-placement and sequential linearization are applied with a fixed α first, and then, the Nelder–Mead method (Nelder and Mead, 1965; Lagarias et al., 1998), which is one of the nonlinear optimization methods, is applied to optimize $\boldsymbol{\rho}$ and α at the same time.

Step 1. Initial guess of α for the first resonance cancellation

The original idea of SRC (Sakata et al., 2014) "cancels" the first resonance mode. The initial guess of α is obtained through an optimization problem to make the gain flat between $\omega_{k_{min}}$ and $\omega_{k_{max}}$, where $\omega_{k_{min}}$ and $\omega_{k_{max}}$ are around the first resonance mode frequency.

$$\underset{\alpha}{\text{minimize}} \quad \|j\omega_k(1-\alpha)P_{v1}(j\omega_k) + j\omega_k\alpha P_{v2}(j\omega_k)\|_\infty \tag{5}$$

$$k \in [k_{min}, k_{max}] \tag{6}$$

$$\text{subject to} \quad 0 \le \alpha \le 1 \tag{7}$$

Step 2. Initial C_{pi} gain calculation by the pole-placement

This section calculates the PI gain by pole-placement for the first order model formulated in (1). A transfer function of the velocity PI controller is

$$C_{pi}(s) = k_{vp} + \frac{k_{vi}}{s}. \tag{8}$$

According to (1) and (8), the controller that places the velocity closed-loop poles of the nominal model (1) at $(s + \omega_v)^2$ is (Goodwin et al., 2000)

$$k_{vp} = 2\omega_v M_n - B_n,\ k_{vi} = \omega_v^2 M_n. \tag{9}$$

The open loop frequency response is $L(j\omega_k, \omega_v) = P(j\omega_k)C(j\omega_k, \omega_v)$. ω_v is maximized by the dichotomy method as follows:

$$\text{maximize} \quad \omega_v \tag{10}$$

$$\text{subject to} \quad r_m - |L(j\omega_k, \omega_v) + \sigma| \le 0,\ {}^\forall k, \tag{11}$$

where $\alpha = \alpha_{src}$. r_m and σ denote the circle condition (Maeda and Iwasaki, 2014) for gain and phase margins. The prohibited circle in the Nyquist plot with a center at $(-\sigma, j0)$ and radius r_m is given by

$$\begin{cases} \sigma &= \dfrac{g_m^2 - 1}{2g_m(g_m \cos\Phi_m - 1)} \\ r_m &= \dfrac{(g_m - 1)^2 + 2g_m(1 - \cos\Phi_m)}{2g_m(g_m \cos\Phi_m - 1)} \end{cases}, \tag{12}$$

where Φ_m and g_m denote the phase and gain margins, respectively.

A designed case referred to as SRC-P-PI (Case 1) skips Steps 3 and 4 and directly applies Step 5.

Step 3. C_{pi} optimization through sequential linearization

Step 3 optimizes C_{pi} through sequential linearization. The gains obtained in Step 2 are used as the initial gains. To linearize the problem, α is fixed as α_{src}.

The controller and open loop frequency responses are given as

$$C_{pi}(j\omega_k, \boldsymbol{\rho}) = \boldsymbol{\rho}^\top \boldsymbol{\phi}(j\omega_k) \tag{13}$$

$$L(j\omega_k, \boldsymbol{\rho}) = P(j\omega_k)C_{pi}(j\omega_k, \boldsymbol{\rho}), \tag{14}$$

where $\boldsymbol{\phi}(j\omega_k) = [1,\ \frac{1}{j\omega_k}]^\top$ denotes the basis function of the controller.

The optimization problem is formulated as

$$\underset{\boldsymbol{\rho}}{\text{maximize}} \quad \Omega_{gc} \tag{15}$$

$$\text{subject to} \quad \left|\frac{\Omega_{gc}}{j\omega_k}\right|^m - |1 + L(j\omega_k, \boldsymbol{\rho})| \le 0,\ {}^\forall k \tag{16}$$

$$r_m - |L(j\omega_k, \boldsymbol{\rho}) + \sigma| \le 0,\ {}^\forall k \tag{17}$$

$$0 \le \boldsymbol{\rho} \tag{18}$$

Ω_{gc} in (15) is a constraint for the sensitivity function in (16). Ω_{gc} denotes a 0 dB cross-over frequency of the sensitivity function. By maximizing Ω_{gc}, the gain of the sensitivity function in the low-frequency range is minimized. Equation (17) is the circle condition of the gain and phase margins. Equation (18) is a constraint to obtain a stable controller.

Equations (16) and (17) are the differences in convex functions and they are not convex. However, by applying a linearization around the current solution point, the new feasible set becomes

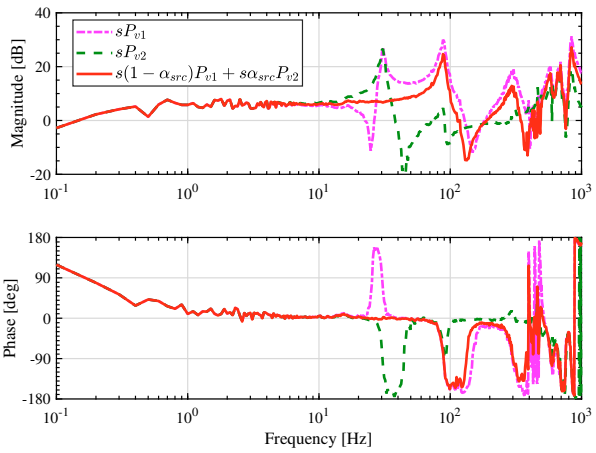

Fig. 4. Initial value of α for SRC determined by the optimization (5)–(7).

a convex subset of the original feasible set (Yuille and Rangarajan, 2003; Hast et al., 2013; Nakamura et al., 2016). Equations (16) and (17) are relaxed as

$$\left|\frac{\Omega_{gc}}{j\omega_k}\right|^m - \Re\left(\frac{(L_j(j\omega_k, \boldsymbol{\rho}_j) + 1)^*}{|L_j(j\omega_k, \boldsymbol{\rho}_j) + 1|}(L(j\omega_k, \boldsymbol{\rho}) + 1)\right) \le 0, \tag{19}$$

$$r_m - \Re\left(\frac{(L_j(j\omega_k, \boldsymbol{\rho}_j) + \sigma)^*}{|L_j(j\omega_k, \boldsymbol{\rho}_j) + \sigma|}(L(j\omega_k, \boldsymbol{\rho}) + \sigma)\right) \le 0 \tag{20}$$

where $\Re$ and * denote the real part and complex conjugate respectively. $L_j(j\omega_k, \boldsymbol{\rho}_j)$ denotes the open loop frequency response of the previous iteration. Therefore, by iterating the procedure, the solution will converge to a saddle point or a local minimum. This procedure is referred to as the concave–convex procedure (CCCP) (Yuille and Rangarajan, 2003).

Ω_{gc} itself is maximized by a dichotomy method. The feasibility problem is solved by YALMIP (Löfberg, 2004) and MOSEK (MOSEK ApS, 2017).

A designed case referred to as SRC-P-PI (Case 2) skips Step 4 and directly applies Step 5.

Step 4. Nonlinear optimization through the Nelder–Mead method

Step 4 applies the Nelder–Mead method to optimize C_{pi} and α at the same time by the following optimization problem:

$$\underset{\boldsymbol{\rho},\alpha}{\text{maximize}} \quad \Omega_{gc} \tag{21}$$

$$\text{subject to} \quad \left|\frac{\Omega_{gc}}{j\omega_k}\right|^m - |1 + L(j\omega_k, \boldsymbol{\rho}, \alpha)| \le 0,\ {}^\forall k \tag{22}$$

$$r_m - |L(j\omega_k, \boldsymbol{\rho}, \alpha) + \sigma| \le 0,\ {}^\forall k \tag{23}$$

$$0 \le \boldsymbol{\rho} \tag{24}$$

$$0 \le \alpha \le 1 \tag{25}$$

The C_{pi} gains obtained in Step 3 and α_{src} obtained in Step 1 are used as the initial values for the Nelder–Mead method.

The optimized α by the Nelder–Mead method is denoted as α_{opt}. A designed case referred to as SRC-P-PI (Case 3) applies Step 5 after Step 4.

Step 5. C_p maximization by dichotomy method

This step optimizes the outer loop position controller $C_p = k_{pp}$. The open loop frequency response of the position controller

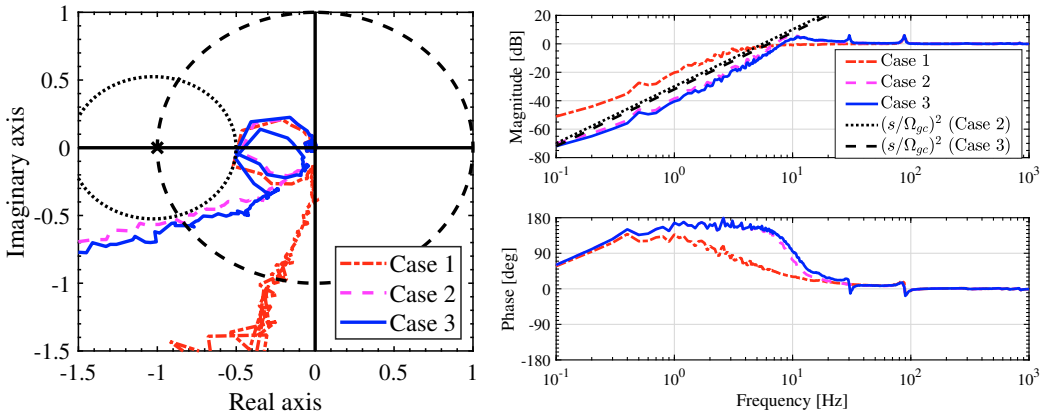

(a) Nyquist plot. (b) Sensitivity function.

Fig. 5. Design results of the velocity loop (SRC-P-PI control).

$L_p(j\omega, k_{pp})$ is formulated as

$$L_p(j\omega_k, k_{pp}) = k_{pp} \frac{C_{pi}(j\omega_k)\frac{P_{v2}(j\omega_k)}{j\omega_k}}{1 + L_{vsrc}(j\omega_k, \boldsymbol{\rho}, \alpha)} \tag{26}$$

k_{pp} is maximized by the dichotomy method with the following optimization:

$$\text{maximize} \quad k_{pp} \tag{27}$$

$$\text{subject to} \quad r_m - |L_p(j\omega_k, k_{pp}) + \sigma| \leq 0, \ {}^\forall k \tag{28}$$

4. EXPERIMENTAL VALIDATION

Experiments are performed using the high-precision positioning stage shown in Fig. 1. The gain and phase margins are set as 6 dB and 30°, respectively. m in (16) is set as 2. The sampling period is set as 400 μs, and the 1 A input disturbance is applied at $t = 0.0$ s.

4.1 Design results of the proposed method

In Step 1, the optimal α, which minimizes the gain of the first resonance mode, is obtained as $\alpha_{src} = 0.484$. According to Fig. 2, $\omega_{k_{min}} = 22.4 \times 2\pi$ [rad/s] and $\omega_{k_{max}} = 32.6 \times 2\pi$ [rad/s]. A frequency response of the plant with SRC is shown in Fig. 4; this shows that the gain and phase characteristics are almost flat between $\omega_{k_{min}}$ and $\omega_{k_{max}}$.

The design results of SRC-P-PI control are shown in Tab. 1 and Fig. 5. The frequency response from the control input to the velocity is shown in Fig. 6. From Fig. 6, $\alpha = \alpha_{opt}$ in SRC-P-PI (Case 3) results in incomplete cancellation of the first resonance. This is because, according to Fig. 2, the gain of the secondary resonance decreases when α approaches 1. In addition, Fig. 5(a) shows that the circle of the first and second resonances of SRC-P-PI (Case 3) have the same radius. As a result, the bandwidth is increased, as shown in Fig. 5(b).

Experimental results of the step disturbance suppression are shown in Fig. 7. According to Fig. 7(a) and Tab. 2, SRC-P-PI (Case 3) shows the best tracking performance in terms of infinity and 2-norm tracking error.

4.2 Initial value dependency of Nelder–Mead method

In the proposed method, the initial value of the Nelder–Mead method is given by the stepwise optimization with the pole placement method and sequential linearization. This section compares the results of the Nelder–Mead method with random initial values to demonstrate the effectiveness of the proposed procedure.

1000 pattern randomly selected values in the range of $0 \leq \alpha \leq 1$, $0 \leq k_{vp} \leq 1$, $0 \leq k_{vi} \leq 10$ are used as the initial values. The optimization results of Ω_{gc} are shown in Fig. 8. The maximum Ω_{gc} case is referred to as "SRC-P-PI (NM1000)". Tab. 1 shows that SRC-P-PI (NM1000) converges a smaller Ω_{gc} when compared to the results of SRC-P-PI (Case 3).

The calculation time of both methods is shown in Tab. 3. NM1000 (Parallel) is calculated using MATLAB's `parfor` to utilize multiple CPU cores. This shows that the proposed method achieves better performance with a shorter calculation time. Moreover, even when using the laptop computer, the proposed method completed the calculation in 26 s, and it is thus also practical in terms of calculation time. Fig. 9 and Tab. 2 show the experimental results of the input disturbance rejection. Tracking performance of SRC-P-PI (Case 3) outperforms that of SRC-P-PI (NM1000).

4.3 Comparison with PID control

This section shows a comparison with PID control shown in Fig. 3(b) to demonstrate the superiority of the controller structure of the SRC-P-PI control. Both design methods use frequency response data and low-order nominal models. The gain margin and phase margin are set as the same as in the SRC-P-PI control 6 dB and 30°, respectively. The weighting m for sensitivity function is set as 3, considering the integrators of the plant and controller. The parameter of the PID controller is optimized through the pole placement method, the sequential linearization method, and the Nelder–Mead method.

Fig. 10 and Tab. 2 show a comparison of the two methods. This indicates that sufficient disturbance suppression performance cannot be obtained only with the non-collocated sensor. The above result shows the superiority of the controller structure of SRC-P-PI control and the effectiveness of the proposed tuning method.

5. CONCLUSION

This paper proposed a tuning method for P-PI control utilizing multiple sensors. An advantage of the proposed method is that

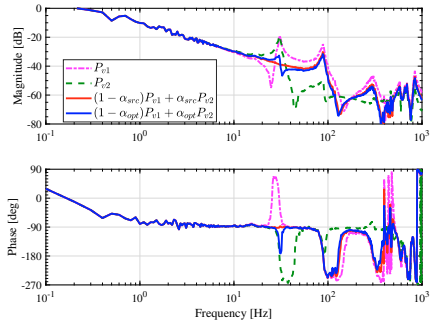

Fig. 6. Frequency response of the plant with SRC.

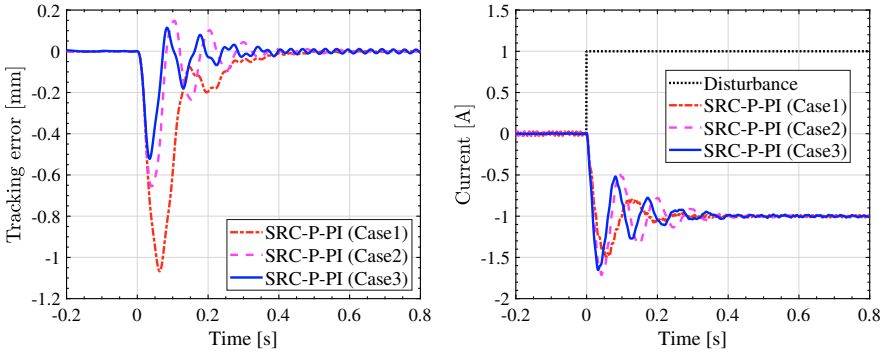

(a) Tracking error. (b) Disturbance and feedback current.

Fig. 7. Experimental results for step disturbance rejection (SRC-P-PI control).

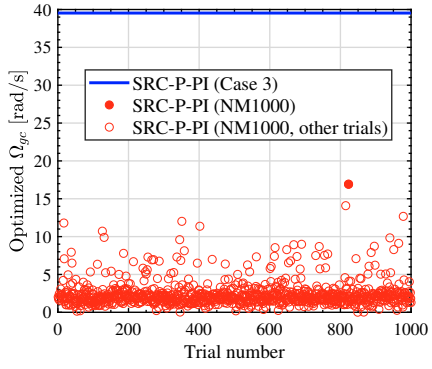

Fig. 8. Optimization results by Nelder–Mead method.

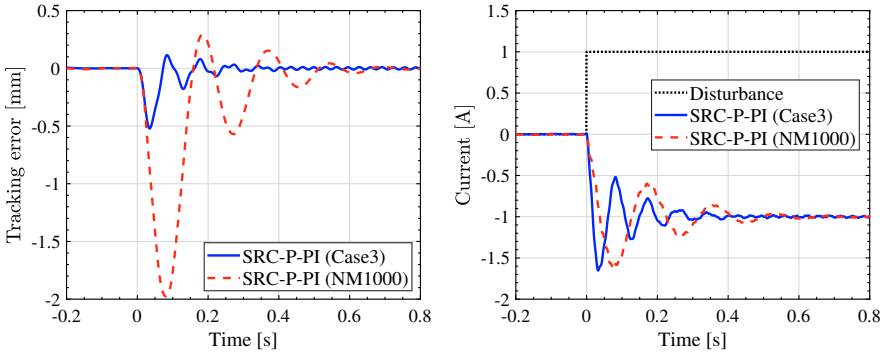

(a) Tracking error. (b) Disturbance and feedback current.

Fig. 9. Experimental results for step disturbance rejection (SRC-P-PI (Case 3, NM1000)).

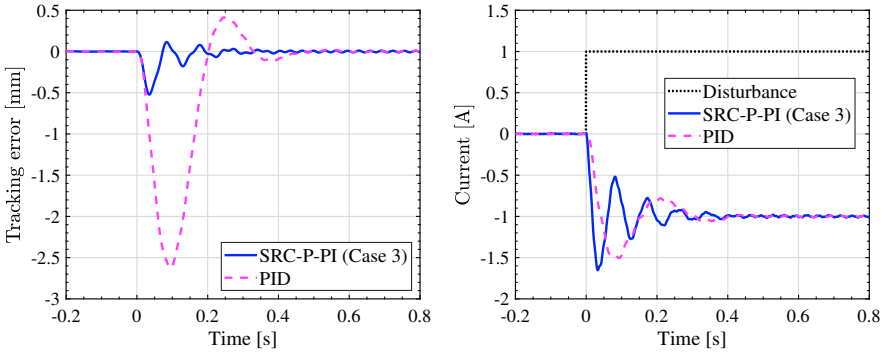

(a) Tracking error. (b) Disturbance and feedback current.

Fig. 10. Experimental results for step disturbance rejection (SRC-P-PI and PID control).

Table 1. Design results (SRC-P-PI control).

	α	k_{vp}	k_{vi}	ω_v, Ω_{gc} [rad/s]	k_{pp}	Note
SRC-P-PI (Case 1)	0.484	17.3	194	ω_v = 21.3	50.4	PP
SRC-P-PI (Case 2)	0.484	15.1	1710	Ω_{gc} = 35.2	16.6	PP→CCCP
SRC-P-PI (Case 3)	0.571	18.8	2160	Ω_{gc} = 39.5	20.3	PP→CCCP→NM
SRC-P-PI (NM1000)	0.0177	9.03	524	Ω_{gc} = 16.9	9.27	See sec. 4.2

PP: Pole Placement, CCCP: Concave–Convex Procedure, NM: Nelder–Mead method

Table 2. Tracking error comparison of the experimental results in mm. Here, () denotes the relative value compared with SRC-P-PI (Case 3).

Methods	$\|e\|_2$	$\|e\|_\infty$
SRC-P-PI (Case 1)	12.7 (2.75)	1.07 (2.05)
SRC-P-PI (Case 2)	6.73 (1.46)	0.656 (1.26)
SRC-P-PI (Case 3)	4.61 (1.00)	0.522 (1.00)
SRC-P-PI (NM1000)	26.5 (5.74)	1.98 (3.78)
PID	37.9 (8.24)	2.63 (5.03)

Table 3. Calculation time comparison.

	Laptop computer	Desktop computer
CPU (# of cores)	Core i7 8550U (4 core)	Core i9 9900K (8 core)
Memory	12GB	48GB
NM1000	13279 [s] (221 [min])	7753 [s] (129 [min])
NM1000 (Parallel)	4764 [s] (79 [min])	1305 [s] (22 [min])
SRC-P-PI (Case 3)	26 [s]	19 [s]

it does not require the high-order parametric model and only utilizes the frequency response data and rigid body nominal model. Hence, the proposed method has the potential to address the plant perturbations and unstructured dynamics by dealing with multiple frequency response data measured under different conditions.

The proposed method employs stepwise optimization with the pole-placement using a nominal model, sequential linearization method, and the Nelder–Mead method. The bandwidth is improved by each step. Further, the proposed procedure obtains high performance with less calculation time compared to the Nelder–Mead method with 1000 pattern random initial values. The effectiveness of the controller structure was demonstrated through comparison with the PID controller optimized by the same procedure.

The proposed method is practical because it requires only frequency response data and a low-order nominal model, and it is applicable with multiple sensors. Considering that systems with multiple encoders are becoming popular, this paper has proposed an effective way to utilize collocated and non-collocated sensors.

REFERENCES

Åström, K.J. and Murray, R.M. (2008). *Feedback Systems: An Introduction for Scientists and Engineers*. Princeton University Press.

Butler, H. (2011). Position Control in Lithographic Equipment. *IEEE Control Systems Magazine*, 31(5), 28–47.

Gaing, Z.L. (2004). A Particle Swarm Optimization Approach for Optimum Design of PID Controller in AVR System. *IEEE Transactions on Energy Conversion*, 19(2), 384–391.

Goodwin, G.C., Graebe, S.F., and Salgado, M.E. (2000). *Control System Design*.

Hara, A., Saiki, K., Sakata, K., and Fujimoto, H. (2008). Basic examination on simultaneous optimization of mechanism and control for high precision single axis stage and experimental verification. In *34th Annual Conference of IEEE Industrial Electronics*, 2509–2514.

Hasegawa, A., Fujimoto, H., and Takahashi, T. (2017). Robot Joint Angle Control Based on Self Resonance Cancellation Using Double Encoders. In *IEEE International Conference on Advanced Intelligent Mechatronics*, 460–465.

Hast, M., Åström, K., Bernhardsson, B., and Boyd, S. (2013). PID Design by Convex-Concave Optimization. In *European Control Conference*, 4460–4465.

Hu, J.s., Hu, F.r., and Kang, C.h. (2014). On the Two-Inertia System: Analysis of the Asymptotic Behaviors to Multiple Feedback Position Control. *Asian Journal of Control*, 16(1), 175–187.

Karimi, A. and Galdos, G. (2010). Fixed-order Hcontroller design for nonparametric models by convex optimization. *Automatica*, 46(8), 1388–1394.

Lagarias, J.C., Reeds, J.A., Wright, M.H., and Wright, P.E. (1998). Convergence Properties of the Nelder–Mead Simplex Method in Low Dimensions. *SIAM Journal on Optimization*, 9(1), 112–147.

Lee, S., Marsolan, N., Sun, T., Lee, S., and Kilian, B. (1985). Application of Self-Optimizing Controllers to Variable Time-Delay Processes. In *American Control Conference*, 1275–1280.

Löfberg, J. (2004). YALMIP : A Toolbox for Modeling and Optimization in MATLAB. In *Proceedings of the CACSD Conference*.

Maeda, Y. and Iwasaki, M. (2014). Circle condition-based feedback controller design for fast and precise positioning. *IEEE Transactions on Industrial Electronics*, 61(2), 1113–1122.

MOSEK ApS (2017). MOSEK Optimization Toolbox for MATLAB 8.1.0.59.

Nakamura, K., Yubai, K., Yashiro, D., and Komada, S. (2016). Controller Design Method Achieving Maximization of Control Bandwidth by Using Nyquist Diagram. In *International Automatic Control Conference*, 35–40.

Nelder, J.A. and Mead, R. (1965). A Simplex Method for Function Minimization. *The Computer Journal*, 7(4), 308–313.

Oomen, T. (2018). Advanced Motion Control for Precision Mechatronics: Control, Identification, and Learning of Complex Systems. *IEEJ Journal of Industry Applications*, 7(2), 127–140.

Pintelon, R. and Schoukens, J. (2012). *System Identification: A Frequency Domain Approach*. Wiley-IEEE Press, 2nd edition.

Sakata, K., Asaumi, H., Hirachi, K., Saiki, K., and Fujimoto, H. (2014). Self Resonance Cancellation Techniques for a Two-Mass System and Its Application to a Large-Scale Stage. *IEEJ Journal of Industry Applications*, 3(6), 455–462.

Tang, K.S., Man, K.F., Chen, G., and Kwong, S. (2001). An optimal fuzzy PID controller. *IEEE Transactions on Industrial Electronics*, 48(4), 757–765.

Yamaguchi, T., Hirata, M., and Pang, J.C.K. (2011). *High-speed precision motion control*.

Yuille, A. and Rangarajan, A. (2003). The Concave-Convex Procedure. *Neural Computation*, 15(4), 915–936.

Ziegler, J.G. and Nichols, N.B. (1942). Optimum settings for automatic controllers. *Transactions of the ASME*, 64(11), 759–768.